

Complete CKM quark mixing via Dimensional Deconstruction

P. Q. Hung*

*Institute for Nuclear and Particle Physics,
and Department of Physics,
University of Virginia,
Charlottesville, Virginia 22904-4714, USA*

A. Soddu†

*Department of Physics,
National Taiwan University,
Taipei, Taiwan 106, R.O.C.*

Ngoc-Khanh Tran‡

*Department of Physics, University of Virginia,
Charlottesville, Virginia 22904-4714, USA*

(Dated: July 13, 2018)

Abstract

It is shown that the deconstruction of $[SU(2) \times U(1)]^N$ into $[SU(2) \times U(1)]$ is capable of providing all necessary ingredients to completely implement the complex CKM mixing of quark flavors. The hierarchical structure of quark masses originates from the difference in the deconstructed chiral zero-mode distributions in theory space, while the CP-violating phase comes from the genuinely complex vacuum expectation value of link fields. The mixing is constructed in a specific model to satisfy experimental bounds on quarks' masses and CP violation.

PACS numbers: 11.25.Mj, 12.15.Ff

*Electronic address: pqh@virginia.edu

†Electronic address: asoddu@hep1.phys.ntu.edu.tw

‡Electronic address: nt6b@virginia.edu

I. INTRODUCTION

Dimensional deconstruction [1], [2] is a very interesting approach to dynamically generate the effects of extra dimensions departing from the four-dimensional (4D) renormalizable physics at ultraviolet scale. That is, apart from having the viability in the sense of renormalizability, whatever amusing mechanisms being dynamically raised by the virtue of extra dimensions (ED) now can also be easily arranged to rise dynamically in a pure 4D framework. In this paper we look specifically into two such important mechanisms of extra dimension theories, namely the localization of matter fields in the bulk [3, 4, 5] and the dynamical breaking of CP symmetry by ED Wilson line [6, 7, 8, 9]. Ultimately, the hybrid of these two mechanisms is just the well-known complex mixing of fermion flavors. And it is conceptually interesting to note that dimensional deconstruction (DD) nicely encompasses both of these issues. In other words, complete Cabibbo-Kobayashi-Maskawa (CKM) mixing can be generated naturally via dimensional deconstruction.

With the presence of extra dimensions, one has a new room to localize the matter fields differently along the transverse directions as in the so-called split fermion scenario. Various overlaps of fermions of different flavors then induce various fermion masses observed in nature (see e.g. [10, 11, 12]). Amazingly, the deconstruction interaction is also able to produce similar localization effects [13]. Indeed, after the spontaneous breaking of link fields, fermions get an extra contribution to their masses via the Higgs mechanism. Fermions then reorganize themselves into mass sequences and the lightest mass eigenstate of these towers exposes some interesting “localization” pattern in the theory space (also referred to as deconstruction group index space). We will first work out the analytical expressions and confirm the localization of these zero modes in a rather generic deconstruction set-up. The next question to raise is how to make these light modes chiral. Imposing some kind of chiral boundary conditions [2] is the answer again coming from the ED lessons. There is however one more subtle point to be mentioned here. If one truly wishes to relate the ED scenario to the dimensional deconstruction, one needs to latticize the extra dimensions to host the deconstruction group. There comes the lattice theory’s issue of fermion doubling, and its standard remedy, such as adding to the Lagrangian a Wilson term [14] would remove half of original chiral degrees of freedom. This is the reason why most of previous works addressing the fermionic mixing in deconstructed picture (e.g. [2, 13, 15]) usually start out with only

Weyl spinors. In the current work, we adopt a different and somewhat more general 4D deconstruction approach [16] where no extra dimension is actually invoked. As a result the fermions to begin with keep a standard 4-component Dirac spinor representation.

In any deconstruction set-up, the link fields transform non-trivially under at least two different gauge groups. This implies a complex vacuum expectation value (VEV) for these fields, whose phase would not be rotated away in general. After the deconstruction process, this phase is carried over into the complex value of wave functions and wave function overlaps of fermions. In turn, the induced complex-valued mass matrices can render a required CP-violating phase in the well-known KM mechanism. In contrast, we note that the generation of complex mass matrices within the split fermion scenario is a non-trivial problem and requires rather sophisticated techniques to solve [17, 18]. Interestingly, the above CP violation induction via deconstruction can also be visualized in extra dimensional view point. Indeed, because of having the same symmetry transformation property, DD link field can be identified with the Wilson line pointing along a latticized transverse direction (Appendix B), and the latter then can naturally acquire a complex VEV in the generalized Hosotani’s mechanism [6, 7, 8, 9] of dynamical symmetry breaking. Apparently, the source of CP violation in this approach comes from the complex effective Yukawa couplings so it can be classified as hard CP violation. Nevertheless, those couplings acquire complex values after the spontaneous breaking of the DD link fields. In that sense this CP violation pattern could also be considered soft and dynamical.

This paper is presented in the following order. In Sec. IIA we give the zero mass eigenstate of fermions obtained in the deconstructed picture, in Sec. IIB the resulting expression of mass matrix elements, and in Sec. IIC the symmetry breaking of $[SU(2) \times U(1)]^N$ into $[SU(2) \times U(1)]$. In Sec. III we present the numerical fit for quark mass spectrum and CKM matrix in a model where each “standard model” Higgs field is chosen to transform under only a single deconstruction subgroup. The conclusion and comments on numerical results is given in Sec. V. Appendix A provides a detailed derivation of zero mode wave functions in 4D deconstruction using combinatoric techniques. Appendix B outlines intuitive arguments on the complexity of link field inspired by lattice models. Appendix C presents analytical expressions for wave function overlaps used in the determination of mass matrix elements. Finally, Appendix D gives referencing values of key physical quantities that have been used in the search algorithm (Table I), and numerical solution of our models’ parameters (Table

II).

II. DECONSTRUCTION AND QUARK MASS MATRIX

In this section we describe how the mixing of quark flavors arises in the DD picture. But we first briefly recall the basic idea of the dimensional deconstruction applied to just a single quark generation. The family replication will be restored in the later sections.

A. Zero-mode fermion

We begin with N copies of gauge group $[SU(2) \times U(1)]_n$ where $n = 1, \dots, N$. To each group $[SU(2) \times U(1)]_n$ we associate a $SU(2)_n$ -doublet Q_n , and two $SU(2)_n$ -singlets U_n, D_n . These fields transform non-trivially only under their corresponding group $[SU(2) \times U(1)]_n$ as $(2, q_Q), (1, q_U), (1, q_D)$ respectively, with q 's denoting $U(1)$ -charges. Finally, we use $3(N-1)$ scalars $\phi_{n-1,n}^Q, \phi_{n-1,n}^U, \phi_{n-1,n}^D$ transforming respectively as $(2, q_Q|2, -q_Q), (1, q_U|1, -q_U), (1, q_D|1, -q_D)$ under $[SU(2) \times U(1)]_{n-1} \times [SU(2) \times U(1)]_n$ to “link” fermions of the same type. Because of this, scalars ϕ 's are also referred to as link fields hereafter. For the simplicity of the model, we assume a symmetry for the Lagrangian under the permutation of group index n .

The $\prod_{n=1}^N [SU(2) \times U(1)]_n$ gauge-invariant Lagrangian of the fermionic sector is

$$\mathcal{L} = \left(\sum_{n=1}^N \bar{Q}_n i \mathcal{D}_n Q_n + \sum_{n=1}^{N-1} \bar{Q}_n \phi_{n,n+1}^Q Q_{n+1} - M_Q \sum_{n=1}^N \bar{Q}_n Q_n \right) + (Q \leftrightarrow U) + (Q \leftrightarrow D), \quad (1)$$

where \mathcal{D}_n denotes the covariant derivative associated with gauge group $[SU(2) \times U(1)]_n$, and M_Q, M_U, M_D are the bare masses of fermions. Ultimately, we are interested in achieving chiral fermions of standard model (SM) at low energy scale. To this aim we impose the following chiral boundary conditions (CBC) on fermion fields [2].

$$\begin{aligned} Q_{1R} = Q_{NR} = 0, & \quad \phi_{N-1,N}^Q Q_{N,L} = V_Q Q_{N-1,L}, \\ U_{1L} = U_{NL} = 0, & \quad \phi_{N-1,N}^U U_{N,R} = V_U U_{N-1,R}, \\ D_{1L} = D_{NL} = 0, & \quad \phi_{N-1,N}^D D_{N,R} = V_D D_{N-1,R}. \end{aligned} \quad (2)$$

We note that those conditions are in agreement with the gauge transformation property of fields, e.g. $\phi_{N-1,N}^Q Q_{N,L}$ and $Q_{N-1,L}$ transform identically under the underlying gauge groups.

zero modes of fermions, we will work only with $[M_Q^\dagger M_Q]$, $[M_U M_U^\dagger]$, $[M_D M_D^\dagger]$ in what follows.

$$[M_Q^\dagger M_Q] = \begin{pmatrix} |V_Q|^2 & -M_Q V_Q & V_Q^2 & 0 \\ -M_Q V_Q^* & M_Q^2 + |V_Q|^2 & -2M_Q V_Q & V_Q^2 \\ (V_Q^*)^2 & -2M_Q V_Q^* & M_Q^2 + 2|V_Q|^2 & -2M_Q V_Q \\ 0 & (V_Q^*)^2 & -2M_Q V_Q^* & M_Q^2 + 2|V_Q|^2 \\ \vdots & \vdots & \vdots & \vdots \\ -2M_Q V_Q^* & M_Q^2 + 2|V_Q|^2 & -2M_Q V_Q & V_Q^2 \\ (V_Q^*)^2 & -2M_Q V_Q^* & M_Q^2 + 2|V_Q|^2 & -2M_Q V_Q + |V_Q|^2 \\ 0 & (V_Q^*)^2 & -2M_Q V_Q^* + (V_Q^*)^2 & M_Q^2 + 2|V_Q|^2 - (V_Q + V_Q^*)M_Q \end{pmatrix}, \quad (6)$$

and similar expressions hold for $[M_U M_U^\dagger]$, $[M_D M_D^\dagger]$. The quantitative derivation of the zero-eigenstates, which are identified with the SM chiral fermion, is presented in appendix A. In this section we just concentrate on some qualitative discussion. In general the diagonalization of matrices (6) leads to the transformation between gauge eigenstates Q_{nL} and mass eigenstates \tilde{Q}_{mL}

$$Q_{nL} = [\mathcal{U}_Q]_{nm} \tilde{Q}_{mL}, \quad \tilde{Q}_{nL} = [\mathcal{U}_Q]_{mn}^* Q_{mL}, \quad (7)$$

where the matrix $[\mathcal{U}_Q]$ diagonalizes $[M_Q^\dagger M_Q]$

$$[M_Q^\dagger M_Q]_{diag} = [\mathcal{U}_Q]^\dagger [M_Q^\dagger M_Q] [\mathcal{U}_Q]. \quad (8)$$

The key observation, which will be analyzed in more details in appendix B, is that VEV $V_{Q,U,D}$ are generically complex and $[\mathcal{U}_{Q,U,D}]$ are truly unitary (i.e. not just orthogonal). This in turn gives non-trivial phases to zero-mode fermions $\tilde{Q}_{0L}, \tilde{U}_{0L}, \tilde{D}_{0L}$ in Eq. (7) and after the SM spontaneous symmetry breaking the obtained mass matrices are complex. Further, the explicit solution of zero mode \tilde{Q}_{0L} (and $\tilde{U}_{0R}, \tilde{D}_{0R}$) in the mass eigenbasis exhibits a very interesting ‘‘localization’’ pattern in the group index space n (see Appendix A). This in turn can serve to generate the mass hierarchy among fermion families in a manner similar to that of ED split fermion scenario (see e.g. [12, 18]). Thus we see that dimensional deconstruction indeed provides all necessary ingredients to construct a complete (complex) CKM structure of fermion family mixing.

B. Complex Mass Matrix

In order to give mass to the above chiral zero-mode of fermions, we introduce Higgs doublet fields just as in the SM. In the simplest and most evident scenario (see [15]), there is one doublet Higgs H_n transforming as $(2, q_Q - q_D \equiv q_U - q_Q)$ under each $[SU(2) \times U(1)]_n$ group. We also implement the replication of families by incorporating family indices $i, j = 1, \dots, 3$. Another scenario to generate the (vector-like) fermion mass hierarchy by assuming various link fields to connect arbitrary sites of the latticized fifth dimension has been proposed in [19].

The gauge-invariant Yukawa terms read

$$\kappa_{ij}^U \sum_{n=1}^N \bar{Q}_n^{(i)} i\sigma_2 H_n^* U_n^{(j)} + \kappa_{ij}^D \sum_{n=1}^N \bar{Q}_n^{(i)} H_n D_n^{(j)} + H.c. . \quad (9)$$

In order to extract the terms involving zero modes, which are the only terms relevant at low energy limit, we rewrite (9) in the mass eigenbasis. However, this procedure depends explicitly on the specific CBCs being imposed on each of the fields Q, U, D. To be generic, let us consider the following configuration. We assume the ‘‘localization’’ of zero modes \tilde{Q}_{0L} , \tilde{U}_{0R} and \tilde{D}_{0R} to be at $n = 1$, $n = 1$ and $n = N$ respectively. To achieve this localization pattern, we impose the following CBCs on these fields (see Eq. (2) and Appendix A, Eq. (A22))

$$\begin{aligned} Q_{1R}^{(i)} = Q_{NR}^{(i)} = 0, & \quad \phi_{N-1,N}^{(i)Q} Q_{NL}^{(i)} = V_Q^{(i)} Q_{N-1L}^{(i)}, \\ U_{1L}^{(j)} = U_{NL}^{(j)} = 0, & \quad \phi_{N-1,N}^{(j)U} U_{NR}^{(j)} = V_U^{(j)} U_{N-1R}^{(j)}, \\ D_{1L}^{(k)} = D_{NL}^{(k)} = 0, & \quad \phi_{1,2}^{(k)D^\dagger} D_{1R}^{(k)} = V_D^{(k)*} D_{2R}^{(k)}. \end{aligned} \quad (10)$$

Because of these boundary conditions, zero modes \tilde{Q}_{0L} , \tilde{U}_{0R} and \tilde{D}_{0R} would be localized at $n = 1$, $n = 1$ and $n = N$ respectively, this also means that the first term of Eq. (9) would represent the overlap between 2 wave function localized at the same site $n = 1$, while the second term represents the overlap between wave functions localized at $n = 1$ and $n = N$. Using (10) to eliminate the dependent components and after the SM spontaneous symmetry breaking $\langle H_n \rangle = (0, v/\sqrt{2})^T$ uniformly for all n 's, we can rewrite the Yukawa term (9) as

$$\begin{aligned} \kappa_{ij}^U \frac{v}{\sqrt{2}} \sum_{i,j=1}^3 \left[\bar{Q}_{1L}^{(i)} U_{1R}^{(j)} + \frac{V_Q^{(i)}}{\phi_{N-1,N}^{(i)Q}} \frac{V_U^{(j)}}{\phi_{N-1,N}^{(j)U}} \bar{Q}_{N-1L}^{(i)} U_{N-1R}^{(j)} + \sum_{n=2}^{N-1} (\bar{Q}_{nL}^{(i)} U_{nR}^{(j)} + \bar{Q}_{nR}^{(i)} U_{nL}^{(j)}) \right] + \\ \kappa_{ij}^D \frac{v}{\sqrt{2}} \sum_{i,k=1}^3 \left[\frac{V_D^{(k)*}}{\phi_{1,2}^{(k)D^\dagger}} \bar{Q}_{1L}^{(i)} D_{2R}^{(k)} + \frac{V_Q^{(i)}}{\phi_{N-1,N}^{(i)Q}} \bar{Q}_{N-1L}^{(i)} D_{NR}^{(k)} + \sum_{n=2}^{N-1} (\bar{Q}_{nL}^{(i)} D_{nR}^{(k)} + \bar{Q}_{nR}^{(i)} D_{nL}^{(k)}) \right]. \quad (11) \end{aligned}$$

After going to the mass eigenbasis by the virtue of transformation of the type (7), keeping only zero-mode terms and together with the assumption of universality for the Yukawa couplings in the up and down sectors, we obtain the following effective mass terms

$$\sum_{i,j=1}^3 \tilde{Q}_{0L}^{(i)} M_{ij}^u \tilde{U}_{0R}^{(j)} + \sum_{i,k=1}^3 \tilde{Q}_{0L}^{(i)} M_{ik}^d \tilde{D}_{0R}^{(k)}, \quad (12)$$

with

$$M_{ij}^u = \kappa_U \frac{v}{\sqrt{2}} \left[\left(\sum_{n=1}^{N-2} [\mathcal{U}_Q^{(i)}]_{n,0}^* [\mathcal{U}_U^{(j)}]_{n,0} \right) + \left(1 + \frac{V_Q^{(i)}}{\phi_{N-1,N}^{(i)Q}} \frac{V_U^{(j)}}{\phi_{N-1,N}^{(j)U}} \right) [\mathcal{U}_Q^{(i)}]_{N-1,0}^* [\mathcal{U}_U^{(j)}]_{N-1,0} \right], \quad (13)$$

$$M_{ik}^d = \kappa_D \frac{v}{\sqrt{2}} \left[\left(\frac{V_D^{(k)*}}{\phi_{1,2}^{(k)D\dagger}} [\mathcal{U}_Q^{(i)}]_{1,0}^* + [\mathcal{U}_Q^{(i)}]_{2,0}^* \right) [\mathcal{U}_D^{(k)}]_{2,0} \right. \\ \left. + \left(\sum_{n=3}^{N-2} [\mathcal{U}_Q^{(i)}]_{n,0}^* [\mathcal{U}_D^{(k)}]_{n,0} \right) + [\mathcal{U}_Q^{(i)}]_{N-1,0}^* \left([\mathcal{U}_D^{(k)}]_{N-1,0} + \frac{V_Q^{(i)}}{\phi_{N-1,N}^{(i)Q}} [\mathcal{U}_D^{(k)}]_{N,0} \right) \right]. \quad (14)$$

Because all $[\mathcal{U}_Q]$, $[\mathcal{U}_U]$, $[\mathcal{U}_D]$ are unitary, the mass matrices M^u , M^d are generally complex. Thus in this simplest deconstruction approach, we might better understand the dynamical origin of CP-violation phase in the SM mass matrices. We also note that (13), (14) represent the specific case where \tilde{Q}_{0L} , \tilde{U}_{0R} and \tilde{D}_{0R} are localized at $n = 1$, $n = 1$ and $n = N$ respectively. All other localization configurations can be similarly found. Further, when we replace link fields ϕ 's in (13), (14) by their VEVs following the deconstruction, these mass matrix elements will look much simpler (see (27), (28)).

Before moving on to give explicit expressions of these complex-valued mass matrices in term of zero mode wave functions (appendix A) and perform the numerical fit, let us briefly turn to the breaking pattern of product group $\prod_{n=1}^N [SU(2) \times U(1)]_n$.

C. Deconstructing $[SU(2) \times U(1)]^N$

For the sake of completeness, in this section we will describe the breaking of $[SU(2) \times U(1)]^N$ into the SM $[SU(2) \times U(1)]$ gauge group by giving uniform VEVs to link fields. The transformation and charge structure of fermions and scalar link fields have been defined in the beginning of previous section. To identify the unbroken symmetries following the deconstruction, we look at the covariant derivative and kinetic terms of scalars.

$$D_\mu \phi_{n,n+1}^U = \partial_\mu \phi_{n,n+1}^U - iq_U \frac{g'_0}{2} B_{n\mu} \phi_{n,n+1}^U + iq_U \frac{g'_0}{2} B_{n+1\mu} \phi_{n,n+1}^U, \quad (15)$$

$$D_\mu \phi_{n,n+1}^D = \partial_\mu \phi_{n,n+1}^D - iq_D \frac{g'_0}{2} B_{n\mu} \phi_{n,n+1}^D + iq_D \frac{g'_0}{2} B_{n+1\mu} \phi_{n,n+1}^D. \quad (16)$$

where B_n is the gauge boson associated with $U(1)_n$, while g'_0 is the common gauge coupling for all $U(1)$'s. For abelian groups, the opposite signs of the last two terms in (15) (and also in (16)) originate from the opposite charges of $\phi_{n,n+1}^U$ (and $\phi_{n,n+1}^D$) under $U(1)_n$ and $U(1)_{n+1}$ (so that terms like $\bar{U}_n \phi_{n,n+1}^U U_n$ are gauge-invariant).

For non-abelian groups, the similar sign reversing will hold for terms in the expression of covariant derivatives (see Eq. (21) below), the nature of which also has its root in the gauge invariance of the theory. Indeed, under the Yang-Mills $SU(2)_n \times SU(2)_{n+1}$ gauge tranformation (note that $\phi_{n,n+1}^Q$ is a 2×2 -matrix)

$$\phi_{n,n+1}^Q \rightarrow T_n \phi_{n,n+1}^Q T_{n+1}^\dagger, \quad (17)$$

$$Q_n \rightarrow T_n Q_n, \quad Q_{n+1} \rightarrow T_{n+1} Q_{n+1}, \quad (18)$$

$$\left[\vec{A}_{n\mu} \frac{\vec{\tau}}{2} \right] \rightarrow T_n \left[\vec{A}_{n\mu} \frac{\vec{\tau}}{2} \right] T_n^\dagger - \frac{i}{g_0} (\partial_\mu T_n) T_n^\dagger, \quad (19)$$

$$\left[\vec{A}_{n+1\mu} \frac{\vec{\tau}}{2} \right] \rightarrow T_{n+1} \left[\vec{A}_{n+1\mu} \frac{\vec{\tau}}{2} \right] T_{n+1}^\dagger - \frac{i}{g_0} (\partial_\mu T_{n+1}) T_{n+1}^\dagger. \quad (20)$$

the covariant derivative of $\phi_{n,n+1}^Q$ must be formulated as follows (so that it transforms exactly like $\phi_{n,n+1}^Q$ in (17))

$$\begin{aligned} D_\mu \phi_{n,n+1}^Q &= \partial_\mu \phi_{n,n+1}^Q - (iq_Q \frac{g'_0}{2} B_{n\mu} \phi_{n,n+1}^Q + ig_0 \vec{A}_{n\mu} \frac{\vec{\tau}}{2} \phi_{n,n+1}^Q) \\ &\quad + (iq_Q \frac{g'_0}{2} B_{n+1\mu} \phi_{n,n+1}^Q + ig_0 \phi_{n,n+1}^Q \vec{A}_{n\mu} \frac{\vec{\tau}}{2}). \end{aligned} \quad (21)$$

where \vec{A}_n and T_n are respectively the gauge bosons and some 2×2 -special unitary matrix characterizing the $SU(2)_n$ transformation, while g_0 is the common gauge coupling for all $SU(2)$'s.

After the deconstruction $\phi_{n,n+1}^{U,D} \rightarrow V_{U,D}$, $\phi_{n,n+1}^Q \rightarrow V_Q \cdot \mathbf{1}_{2 \times 2}$, the mass terms for gauge bosons are generated. Specifically, we obtain as parts of kinetic terms $(D_\mu \phi_{n,n+1}^U)^\dagger (D^\mu \phi_{n,n+1}^U)$, $(D_\mu \phi_{n,n+1}^D)^\dagger (D^\mu \phi_{n,n+1}^D)$, $\text{Tr}[(D_\mu \phi_{n,n+1}^Q)^\dagger (D^\mu \phi_{n,n+1}^Q)]$ the following gauge bosons squared mass matrices

$$[M_B^2] = \lambda_B \begin{pmatrix} 1 & -1 & & & \\ -1 & 2 & & & \\ & & \ddots & & \\ & & & 2 & -1 \\ & & & -1 & 1 \end{pmatrix}; \quad [M_{\vec{A}}^2] = \lambda_{\vec{A}} \begin{pmatrix} 1 & -1 & & & \\ -1 & 2 & & & \\ & & \ddots & & \\ & & & 2 & -1 \\ & & & -1 & 1 \end{pmatrix}. \quad (22)$$

where, after restoring the family replication index ($i = 1, 2, 3$),

$$\lambda_B = \sum_1^3 g_0'^2 (q_U^2 |V_U^{(i)}|^2 + q_D^2 |V_D^{(i)}|^2 + q_Q^2 |V_Q^{(i)}|^2), \quad \lambda_{\vec{A}} = \sum_1^3 g_0^2 |V_Q^{(i)}|^2. \quad (23)$$

Both matrices in (22) have a “flat” zero eigenstate. This indeed indicates the uniform breaking of $[SU(2) \times U(1)]^N$ into the diagonal (SM) group $[SU(2) \times U(1)]$, whose gauge bosons are massless and given by

$$\vec{B}_\mu = \frac{1}{\sqrt{N}} \sum_{n=1}^N B_{n\mu}, \quad \vec{A}_\mu = \frac{1}{\sqrt{N}} \sum_{n=1}^N \vec{A}_{n\mu}. \quad (24)$$

In Eq. (23) it is also shown that the pattern of symmetry breaking is not spoiled by family replication as long as charges q_U (and q_D, q_Q) are independent of the site index n under a presumed permutation symmetry (just like $V_{U,D,Q}^{(i)}$). Finally, by extracting the interaction between fermions and massless gauge bosons from fermion kinetic terms in (1) one can see that the couplings of the unbroken group scale as $g' = g_0'/\sqrt{N}$ and $g = g_0/\sqrt{N}$, while the charge structure (of fermions in mass eigenbasis) under this diagonal group remains intact.

III. FITTING THE MODEL'S PARAMETERS

A. Model, Parameters and Numerical Method

In the previous section we have outlined the process diagonalizing the squared-mass matrix (6). The complete diagonalization process is complicated, but as we are concerned only with the zero eigenvalue problem, the computation can be done analytically in the general term (see Appendix A). Since $[\mathcal{U}_Q]$ diagonalizes $[M_Q^\dagger M_Q]$ (8), the zero eigenstate of $[M_Q^\dagger M_Q]$ is just the first column of $[\mathcal{U}_Q]$, i.e. in the notation of appendix A

$$[\mathcal{U}_Q^{(i)}]_{n,0} = x_{Qn}^{(i)}, \quad (25)$$

and similarly

$$[\mathcal{U}_U^{(j)}]_{n,0} = x_{Un}^{(j)}, \quad [\mathcal{U}_D^{(k)}]_{n,0} = y_{Dn}^{(k)}, \quad (26)$$

where x_n 's are given in (A20) (corresponding to a zero mode localized at the end point $n = 1$) and y_n 's in (A24) (corresponding to a zero mode localized at the end point $n = N$).

After the spontaneous symmetry breaking, the link fields acquire an uniform VEV $V_{Q,U,D}$ respectively (independent of site index n). In term of x_n 's and y_n 's, the SM mass matrices

(13), (14) for up and down quark sectors become

$$M_{ij}^u = \kappa_U \frac{v}{\sqrt{2}} \left[\left(\sum_{n=1}^{N-1} x_{Qn}^{(i)*} x_{Un}^{(j)} \right) + x_{QN-1}^{(i)*} x_{UN-1}^{(j)} \right], \quad (27)$$

$$M_{ik}^d = \kappa_D \frac{v}{\sqrt{2}} \left[x_{Q1}^{(i)*} y_{D2}^{(k)} + \left(\sum_{n=2}^{N-1} x_{Qn}^{(i)*} y_{Dn}^{(k)} \right) + x_{QN-1}^{(i)*} y_{DN}^{(k)} \right], \quad (28)$$

where x_n 's, y_n 's are given in (A20), (A24) respectively. The analytical forms of (27), (28) in term of model's parameters are worked out in Appendix C, Eqs. (C1), (C2).

Again, let us remind ourselves that (27) represents the overlap between two wave functions localized at the same site $n = 1$ while (28) represents the overlap between one wave function localized at $n = 1$ and the other at $n = N$. The model under consideration consists of 20 real parameters (see Table II and appendix B): 3 complex VEV V 's for each complete quark generation $(Q, U, D)_i$ ($i=1,2$ or 3), and 2 real "dimensionful" Yukawa couplings $\kappa_U v/\sqrt{2}$, $\kappa_D v/\sqrt{2}$. We choose to fix $N = 10$ throughout.

The numerical approach to fit the parameters consists in minimizing a positive function which gets a zero value when all the predicted quantities are in the corresponding experimental ranges [18]. The minimization procedure is based on the simulated annealing method, which seems working better than other minimization approaches when the parameter space becomes larger [20],[21]. The input referencing physical quantities are given in Table I of Appendix D.

We consider eight different cases, which correspond to all the eight possible ways of localizing the left and right components. The eight different cases are the following:

1. Q , U and D localized in $n = 1$ denoted as ($QU D1$)
2. Q and U localized in $n = 1$, D localized in $n = N$ denoted as ($QU1DN$)
3. Q and D localized in $n = 1$, U localized in $n = N$ denoted as ($QD1UN$)
4. Q localized in $n = 1$, U and D localized in $n = N$ denoted as ($Q1UDN$)
5. Q , U and D localized in $n = N$ denoted as ($QU DN$)
6. D localized in $n = 1$, Q and U localized in $n = N$ denoted as ($D1QU N$)
7. U localized in $n = 1$, Q and D localized in $n = N$ denoted as ($U1QDN$)

8. U and D localized in $n = 1$, Q localized in $n = N$ denoted as $(UD1QN)$

We specially note that, due to the mirror complexity between CBCs (2) and (A22), the mass matrices obtained in the cases 1 and 5, cases 2 and 6, cases 3 and 7, cases 4 and 8, are complex conjugate pairwise. In the result, all eight cases are inequivalent.

B. Numerical results

In the following we present the characteristically important numerical results for the four cases out the eight mentioned above, for which we were able to find solutions. The cases are referred to in the above order. For each case we give one particular, but typical, numerical complete set of the 20 defining parameters (Table II), the quark mass matrices and quark mass spectra, the CKM matrix and the CP parameters. Complex phases are measured in radiant, and $N = 10$ for all cases. The masses are given in GeV and are evaluated at the M_Z scale. For the sake of visualization, we also present graphically the comprehensive solutions of the quark wave function profiles in the theory space (Fig. 1), the mass spectrum (Fig. 2), the CKM matrix (Fig. 3) and the $\bar{\rho}\text{-}\bar{\eta}$ CP parameters (Fig. 4) for the case of all fields Q, U and D localized at the same site $n = 1$.

- Case 1: Q, U and D localized in $n = 1$.

$$M_u^{(QU D1)} = 78.4 \text{ GeV} \begin{pmatrix} 0.925 e^{-0.558 i} & 0.923 e^{-0.501 i} & 0.951 e^{-0.570 i} \\ 0.027 e^{2.009 i} & 0.027 e^{2.046 i} & 0.029 e^{2.006 i} \\ 0.948 e^{0.306 i} & 0.942 e^{0.367 i} & 0.973 e^{0.280 i} \end{pmatrix}, \quad (29)$$

$$m_u^{(QU D1)} = 0.0021 \text{ GeV}, \quad m_c^{(QU D1)} = 0.702 \text{ GeV}, \quad m_t^{(QU D1)} = 181.1 \text{ GeV}, \quad (30)$$

$$M_d^{(QU D1)} = 1.35 \text{ GeV} \begin{pmatrix} 0.909 e^{1.490 i} & 0.782 e^{-2.072 i} & 0.960 e^{0.992 i} \\ 0.030 e^{-2.649 i} & 0.048 e^{0.930 i} & 0.032 e^{-3.025 i} \\ 0.848 e^{2.339 i} & 0.799 e^{-1.353 i} & 0.918 e^{1.838 i} \end{pmatrix}, \quad (31)$$

$$m_d^{(QU D1)} = 0.0045 \text{ GeV}, \quad m_s^{(QU D1)} = 0.106 \text{ GeV}, \quad m_b^{(QU D1)} = 2.89 \text{ GeV}. \quad (32)$$

In Eqs. (29), (31) the mass matrices are written in a form that better shows deviations from the democratic structure. In Eq. (33) we give the expression for the CKM matrix, in Eq. (34) the values for the CP parameters $\bar{\rho}$ and $\bar{\eta}$.

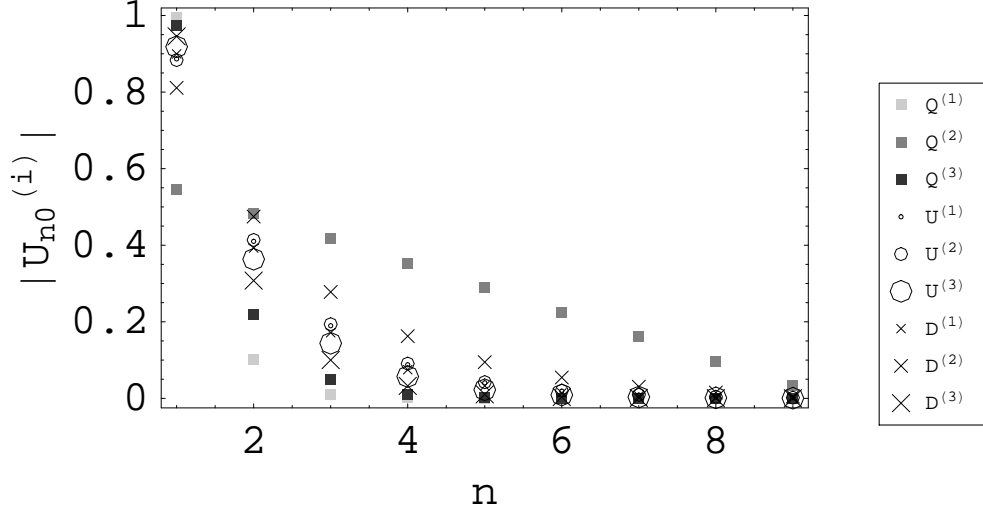


FIG. 1: Profiles of the absolute value of normalized wave functions $|x_{Q_n}^{(i)}|$, $|x_{U_n}^{(i)}|$ and $|x_{D_n}^{(i)}|$ in the theory space ($N=10$) for the case with Q , U and D localized at $n=1$. $|x_{Q_n}^{(2)}|$ with a value of $\alpha \ll 1$ is less localized.

$$V_{CKM}^{(QU D1)} = \begin{pmatrix} 0.975 - 0.009 i & -0.151 - 0.160 i & -0.001 - 0.003 i \\ 0.015 + 0.219 i & -0.669 + 0.709 i & 0.029 + 0.024 i \\ 0.003 - 0.009 i & 0.029 - 0.023 i & 0.670 + 0.742 i \end{pmatrix}, \quad (33)$$

$$\bar{\rho}^{(QU D1)} = 0.12, \quad \bar{\eta}^{(QU D1)} = 0.30, \quad (34)$$

with $\bar{\rho}$ and $\bar{\eta}$ defined as

$$\bar{\rho} = \text{Re}(V_{ud}V_{ub}^*V_{cd}V_{cb}^*)/|V_{cd}V_{cb}^*|^2, \quad (35)$$

$$\bar{\eta} = \text{Im}(V_{ud}V_{ub}^*V_{cd}V_{cb}^*)/|V_{cd}V_{cb}^*|^2. \quad (36)$$

- Case 2: Q and U localized in $n = 1$, D localized in $n = N$.

$$M_u^{(QU1DN)} = 66.6 \text{ GeV} \begin{pmatrix} 0.918 e^{0.039 i} & 0.609 e^{-0.590 i} & 0.924 e^{0.135 i} \\ 0.941 e^{0.038 i} & 0.637 e^{-0.601 i} & 0.946 e^{0.132 i} \\ 0.930 e^{0.058 i} & 0.622 e^{-0.585 i} & 0.935 e^{0.154 i} \end{pmatrix}, \quad (37)$$

$$m_u^{(QU1DN)} = 0.0020 \text{ GeV}, \quad m_c^{(QU1DN)} = 0.687 \text{ GeV}, \quad m_t^{(QU1DN)} = 168.3 \text{ GeV}, \quad (38)$$

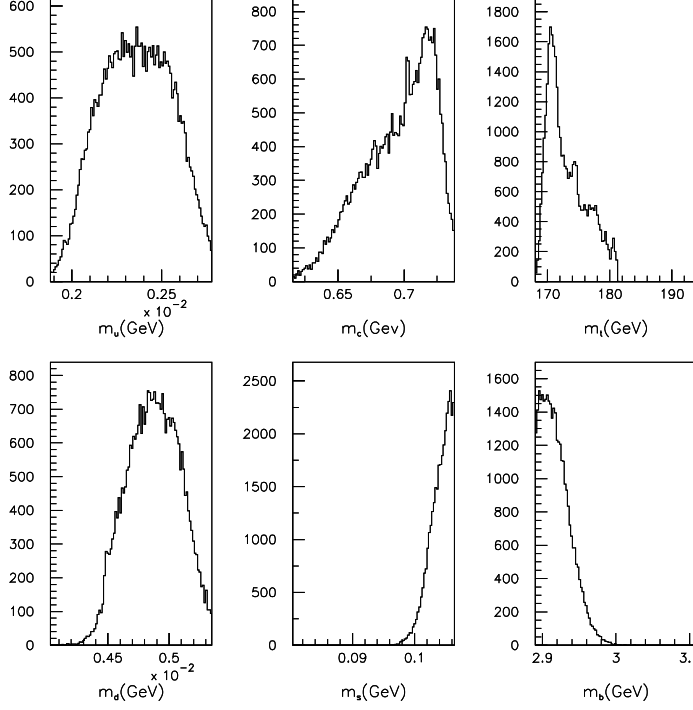


FIG. 2: Solutions for the 6 quark masses in the case with Q , U and D localized at $n=1$. The masses in GeV are evaluated at the M_Z scale. The range for each mass is given by the edges of the corresponding window.

$$M_d^{(QU1DN)} = 23.2 GeV \begin{pmatrix} 0.041 e^{1.959 i} & 0.045 e^{-0.025 i} & 0.043 e^{2.526 i} \\ 0.037 e^{1.854 i} & 0.042 e^{0.003 i} & 0.042 e^{2.570 i} \\ 0.038 e^{1.982 i} & 0.043 e^{0.047 i} & 0.043 e^{2.605 i} \end{pmatrix}, \quad (39)$$

$$m_d^{(QU1DN)} = 0.0045 GeV, \quad m_s^{(QU1DN)} = 0.084 GeV, \quad m_b^{(QU1DN)} = 2.90 GeV, \quad (40)$$

$$V_{CKM}^{(QU1DN)} = \begin{pmatrix} 0.975 + 0.029 i & -0.097 + 0.197 i & 0.001 + 0.003 i \\ -0.168 - 0.141 i & -0.880 + 0.420 i & 0.039 - 0.011 i \\ 0.003 + 0.010 i & 0.039 - 0.007 i & 0.999 + 0.011 i \end{pmatrix}, \quad (41)$$

$$\bar{\rho}^{(QU1DN)} = 0.19, \quad \bar{\eta}^{(QU1DN)} = 0.33. \quad (42)$$

- Case 5: Q , U and D localized in $n = N$.

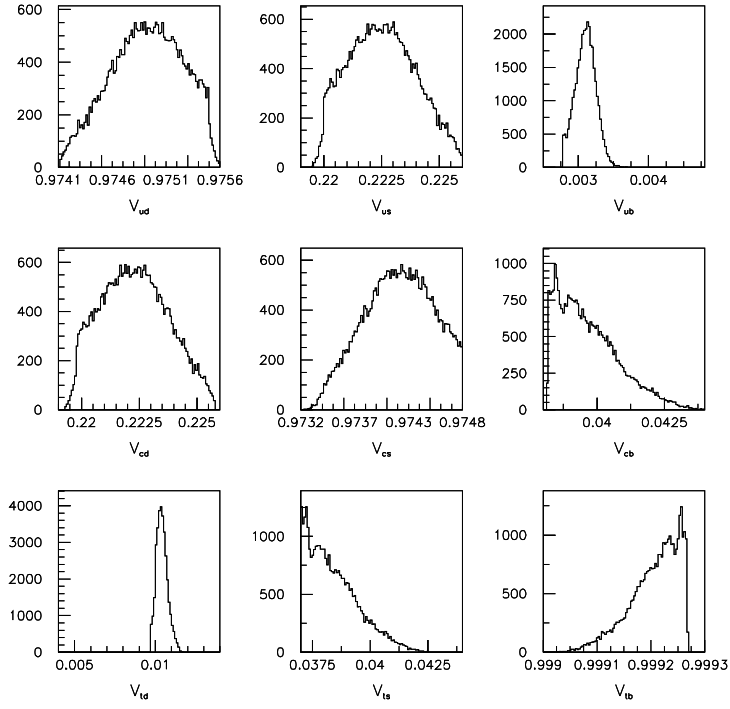


FIG. 3: Solutions for the absolute values of the CKM matrix elements in the case with Q , U and D localized at $n=1$. The range for each element is given by the edges of the corresponding window.

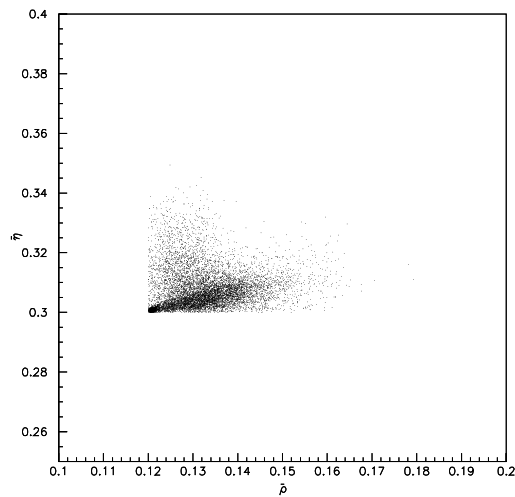


FIG. 4: Solutions for $\bar{\rho}$ and $\bar{\eta}$ in the case with Q , U and D localized at $n=1$.

$$M_u^{(QU DN)} = 78.4 \text{ GeV} \begin{pmatrix} 0.887 e^{0.494 i} & 0.881 e^{0.478 i} & 0.913 e^{0.577 i} \\ 0.038 e^{-2.066 i} & 0.038 e^{-2.070 i} & 0.041 e^{-2.039 i} \\ 0.895 e^{-0.410 i} & 0.877 e^{-0.429 i} & 0.929 e^{-0.316 i} \end{pmatrix}, \quad (43)$$

$$m_u^{(QU DN)} = 0.0022 \text{ GeV}, \quad m_c^{(QU DN)} = 0.674 \text{ GeV}, \quad m_t^{(QU DN)} = 172.6 \text{ GeV}, \quad (44)$$

$$M_d^{(QU DN)} = 1.37 \text{ GeV} \begin{pmatrix} 0.895 e^{-1.619 i} & 0.776 e^{1.668 i} & 0.943 e^{-1.622 i} \\ 0.058 e^{2.456 i} & 0.040 e^{-1.459 i} & 0.063 e^{2.339 i} \\ 0.835 e^{-2.473 i} & 0.832 e^{0.871 i} & 0.893 e^{-2.468 i} \end{pmatrix}, \quad (45)$$

$$m_d^{(QU DN)} = 0.0049 \text{ GeV}, \quad m_s^{(QU DN)} = 0.106 \text{ GeV}, \quad m_b^{(QU DN)} = 2.90 \text{ GeV}, \quad (46)$$

$$V_{CKM}^{(QU DN)} = \begin{pmatrix} 0.974 + 0.042 i & -0.046 + 0.220 i & 0.003 - 0.003 i \\ 0.134 - 0.180 i & -0.676 - 0.701 i & 0.020 - 0.033 i \\ -0.010 + 0.006 i & 0.022 + 0.030 i & 0.646 - 0.762 i \end{pmatrix}, \quad (47)$$

$$\bar{\rho}^{(QU DN)} = 0.31, \quad \bar{\eta}^{(QU DN)} = 0.30. \quad (48)$$

- Case 6: D localized in $n = 1$, Q and U localized in $n = N$.

$$M_u^{(D1QU N)} = 71.2 \text{ GeV} \begin{pmatrix} 0.675 e^{-1.829 i} & 0.824 e^{-0.198 i} & 0.837 e^{-0.732 i} \\ 0.706 e^{-1.783 i} & 0.856 e^{-0.173 i} & 0.868 e^{-0.698 i} \\ 0.671 e^{-1.837 i} & 0.822 e^{-0.207 i} & 0.834 e^{-0.741 i} \end{pmatrix}, \quad (49)$$

$$m_u^{(D1QU N)} = 0.0026 \text{ GeV}, \quad m_c^{(D1QU N)} = 0.725 \text{ GeV}, \quad m_t^{(D1QU N)} = 169.2 \text{ GeV}, \quad (50)$$

$$M_d^{(D1QU N)} = 26.5 \text{ GeV} \begin{pmatrix} 0.026 e^{0.996 i} & 0.039 e^{-3.019 i} & 0.044 e^{-1.678 i} \\ 0.027 e^{0.868 i} & 0.037 e^{-3.017 i} & 0.042 e^{-1.655 i} \\ 0.025 e^{0.957 i} & 0.039 e^{-3.050 i} & 0.044 e^{-1.710 i} \end{pmatrix}, \quad (51)$$

$$m_d^{(D1QU N)} = 0.0044 \text{ GeV}, \quad m_s^{(D1QU N)} = 0.088 \text{ GeV}, \quad m_b^{(D1QU N)} = 2.91 \text{ GeV}, \quad (52)$$

$$V_{CKM}^{(D1QU N)} = \begin{pmatrix} -0.972 - 0.075 i & -0.069 + 0.213 i & 0.001 + 0.004 i \\ -0.050 - 0.218 i & 0.974 + 0.013 i & -0.039 - 0.016 i \\ -0.004 - 0.012 i & 0.038 - 0.014 i & 0.998 + 0.044 i \end{pmatrix}, \quad (53)$$

$$\bar{\rho}^{(D1QU N)} = 0.26, \quad \bar{\eta}^{(D1QU N)} = 0.38. \quad (54)$$

We are now ready for comments on the presented numerical solutions.

IV. CONCLUDING COMMENTS

In this paper we have reconstructed the observed complex mixing of quark flavors, starting with the product group $\prod_{n=1}^N [SU(2) \times U(1)]_n$ at a higher energy scale. The deconstruction of this product group into the electroweak gauge group can indeed provide all necessary components to generate such mixing.

We have built a specific models with 20 parameters to fit the quark mass spectrum and the CP phase. However, the numerical fit is found only for the “preferred” configurations where fermion fields Q and U are localized at the same position in the theory space. Arguably, this is because the ratio κ_U/κ_D of Yukawa couplings can be responsible only for the difference in the overall scale of up and down-quark masses, while the more hierarchical internal mass spectrum of the up-quark sector (compared to that of the down-quark sector) would still require a higher degree of overlapping.

As far as the structure of mass matrices is concerned, the deviation from democracy is moderate. In all the cases, the mass matrices assume a hierarchy with two rows (or two columns) having similar absolute value matrix elements, with the third row (or third column) having different values, but still similar along that row (or that column). A quite close mass matrix structure was found in [18], but in a different approach.

We did not perform a study of the dependence on the number of deconstruction subgroups N . We expect anyway that the fitting would be more feasible for larger N as the wave functions and their overlaps then can be tuned more smoothly. In the other direction, the constraint from flavor changing neutral current that sets an upper limit on the length of extra dimension in the split fermion scenario (see e.g. [23]) is also expected to set an upper limit on the ratio N/V (between N and the VEV of link field) in the deconstruction theory. We however leave a more careful analysis of these and other relevant phenomenological issues for future publications.

Acknowledgments

P.Q.H and N-K.T are supported in part by the U.S. Department of Energy under Grant No. DE-A505-89ER40518. A.S. is supported by grant NSC 93-2811-M-002-047. N-K.T. also acknowledges the Dissertation Year Fellowship from UVA Graduate School of Arts and Sciences.

APPENDIX A: FERMION ZERO MODE IN DIMENSIONAL DECONSTRUCTION

In this appendix we will work out the general expression of zero eigenstate of the matrix of the type (6). This mode plays a special role because it will be identified with the SM chiral fermions. To simplify the writing, here we denote this zero eigenstate generally as $\{x_1, x_2, \dots, x_{N-1}\}$ while in Section III we will restore all omitted scripts Q, U, D, i, j .

1. Zero-mode localization at the end-point $n=1$

The equation set determining the zero eigenstate (6) is

$$|V|^2 x_1 - MVx_2 + V^2 x_3 = 0 \Leftrightarrow V^* x_1 - Mx_2 + Vx_3 = 0 \quad (\text{A1})$$

$$-MV^* x_1 + (M^2 + |V|^2)x_2 - 2MVx_3 + V^2 x_4 = 0 \quad (\text{A2})$$

$$V^{*2} x_1 - 2MV^* x_2 + (M^2 + 2|V|^2)x_3 - 2MVx_4 + V^2 x_5 = 0 \quad (\text{A3})$$

...

$$V^{*2} x_{N-5} - 2MV^* x_{N-4} + (M^2 + 2|V|^2)x_{N-3} - 2MVx_{N-2} + V^2 x_{N-1} = 0 \quad (\text{A4})$$

$$V^{*2} x_{N-4} - 2MV^* x_{N-3} + (M^2 + 2|V|^2)x_{N-2} + (V^2 - 2MV)x_{N-1} = 0 \quad (\text{A5})$$

$$V^{*2} x_{N-3}(V^{*2} - 2MV^*)x_{N-2} + [M^2 - M(V + V^*) + 2|V|^2]x_{N-1} = 0. \quad (\text{A6})$$

After a bit of algebra, we can equivalently transform this equation set into

$$X_1 = X_2 - |\rho|^2 X_3 \quad (\text{A7})$$

$$X_2 = X_3 - |\rho|^2 X_4 \quad (\text{A8})$$

...

$$X_{N-3} = X_{N-2} - |\rho|^2 X_{N-1} \quad (\text{A9})$$

$$X_{N-2} = X_{N-1} - \rho X_{N-1}, \quad (\text{A10})$$

where we have introduced new parameter and variables

$$\rho \equiv |\rho|e^{i\theta} \equiv \frac{V}{M} = \frac{|V|e^{i\theta}}{M} \quad (\text{A11})$$

$$X_n \equiv (\rho^*)^{N-n-1} x_n \quad (n = 1, \dots, N-1). \quad (\text{A12})$$

We note that V (and ρ) is a complex parameter in general (see appendix B). The new simple recursion relation allows us to analytically determine the set $\{X_1, \dots, X_{N-1}\}$ (and then the zero eigenstate $\{x_1, \dots, x_{N-1}\}$) for any ρ (i.e. for any real M and complex V). After some combinatorics [25] we obtain for $1 \leq n \leq N-3$

$$\begin{aligned} X_n &= \quad (\text{A13}) \\ &= \sum_{k=0} \binom{N-3-n-k}{k} (-|\rho|^2)^{k+1} X_{N-1} + \sum_{k=0} \binom{N-2-n-k}{k} (-|\rho|^2)^k X_{N-2} \\ &= \sum_{k=0} \frac{(N-3-n-k)!}{k!(N-3-n-2k)!} (-|\rho|^2)^{k+1} X_{N-1} + \sum_{k=0} \frac{(N-2-n-k)!}{k!(N-2-n-2k)!} (-|\rho|^2)^k X_{N-2}, \end{aligned}$$

and for $n = N-2$ (see (A10))

$$X_{N-2} = (1 - \rho)X_{N-1}. \quad (\text{A14})$$

Using the equality

$$\binom{m}{p} + \binom{m}{p+1} = \binom{m+1}{p+1}, \quad (\text{A15})$$

we can rewrite (A13) as (with $1 \leq n \leq N-3$)

$$X_n = \left[\sum_{k=0} \binom{N-1-n-k}{k} (-|\rho|^2)^k - \rho \sum_{k=0} \binom{N-2-n-k}{k} (-|\rho|^2)^k \right] X_{N-1}. \quad (\text{A16})$$

Again, using another equality [24]

$$\sinh px = \sinh x \sum_{k=0} (-1)^k \binom{p-1-k}{k} (2 \cosh x)^{p-1-2k}, \quad (\text{A17})$$

we obtain for $1 \leq n \leq N-3$ and for $|\rho| < \frac{1}{2}$

$$X_n = \frac{2X_{N-1}}{\sqrt{1-4|\rho|^2}} \left[|\rho|^{N-n} \sinh(N-n)\alpha - \rho |\rho|^{N-1-n} \sinh(N-1-n)\alpha \right], \quad (\text{A18})$$

with

$$\cosh \alpha \equiv \frac{1}{2|\rho|} \Leftrightarrow \alpha \equiv \cosh^{-1} \frac{1}{2|\rho|} \quad (\alpha > 0). \quad (\text{A19})$$

For $|\rho| > \frac{1}{2}$, the expression of X_N is similar to (A18) but with hyperbolic functions (\sinh and \cosh) replaced respectively by trigonometric ones (\sin and \cos).

Finally, from (A12) we have altogether

$$x_n = C e^{-in\theta} \left[\sinh(N-n)\alpha - e^{i\theta} \sinh(N-1-n)\alpha \right] \quad (1 \leq n \leq N-1), \quad (\text{A20})$$

where C is the normalization constant determined by the normalization equation

$$\sum_{n=1}^{N-1} |x_n|^2 = 1. \quad (\text{A21})$$

We note that this normalization is nothing other than the unitarity condition of the rotation matrix \mathcal{U} (see (8) and (25), (26)).

2. Zero-mode localization at the end-point $n=N$

The chiral boundary conditions (CBC) and the value of parameter $|\rho| \equiv |V|/|M|$ are two crucial factors that determine the localization pattern of the chiral zero-mode of fermion. For e.g. in the previous subsection we have seen that, when $|\rho| < 1/2$, along with CBCs $Q_{1R} = Q_{NR} = 0$, $\phi_{N-1,N}^Q Q_{N,L} = V_Q Q_{N-1,L}$ (2) we can localize the left-handed zero mode of Q field around site $n = 1$ (A20).

On the intuitive ground, we expect that the ‘‘mirror image’’ of (2) (apart from the requirement $|\rho| < 1/2$)

$$Q_{1,R} = Q_{N,R} = 0, \quad \phi_{1,2}^{Q\dagger} Q_{1,L} = V_Q^* Q_{2,L}, \quad (\text{A22})$$

would produce a left-handed zero mode of Q field localized at $n = N$. A similar calculation indeed confirms this localization pattern. Specifically, if we denote y_i ($i = 2, \dots, N$) the zero-mode subject to CBCs (A22), and x_j ($j = 1, \dots, N-1$) subject to CBCs (2) as before, we find

$$y_i = x_{N+1-i}^* \quad (i = 2, \dots, N), \quad (\text{A23})$$

or even more explicitly (see (A20))

$$y_n = C e^{i(N+1-n)\theta} \left[\sinh(n-1)\alpha - e^{-i\theta} \sinh(n-2)\alpha \right] \quad (2 \leq n \leq N). \quad (\text{A24})$$

APPENDIX B: THE COMPLEX-VALUED LINK FIELD VEV FROM BROKEN WILSON LINE

Since the link fields $\phi_{n,n+1}$ transform non-trivially under two different groups, we may expect its VEV to be complex in general. It is because in this case the VEV's phase could not be rotated away in general. The standard and rigorous method to determine the VEV is to write down and then minimize the corresponding potential. It turns out [22] that there always exist ranges of potential parameters which generate complex VEV. In this appendix, however, we just recapitulate the complexity nature of link field VEV from the latticized extra dimension perception which is derived in [14] in details. Though the approach taken in this work does not strictly stem from latticizing the fifth dimension, this perception could still serve as the principle illustration.

To make the connection between DD theory and its latticized ED counterpart, we interpret the link field as a Wilson line connecting two neighboring branes

$$\phi_{n,n+1} \sim \exp\left(\int_{na}^{(n+1)a} ig\chi_y dy\right) \sim \exp(iga\chi_n), \quad (\text{B1})$$

where χ_n essentially is the ED component of gauge field, g and a are gauge coupling and lattice spacing respectively.

Following the DD symmetry breaking $[SU(2) \times U(1)]^N \rightarrow [SU(2) \times U(1)]$, only one linear combination χ_0 of link fields remains massless at the classical level

$$\chi_0 = \frac{1}{\sqrt{N}} \sum_{n=1}^N \chi_n. \quad (\text{B2})$$

In the leading order with radiative correction, by minimizing the 1-loop effective potential of χ_0 , one obtains [26]

$$\langle \chi_0 \rangle = \frac{2\pi k}{ga\sqrt{N}} \quad (k \in N). \quad (\text{B3})$$

From (B1), (B2), one see that in the leading order the link fields assume a uniform complex VEV

$$\langle \phi_{n,n+1} \rangle \sim \exp\left(\frac{i2k\pi}{N}\right). \quad (\text{B4})$$

Actually, this phase can be considered arbitrary.

APPENDIX C: WAVE FUNCTION OVERLAP IN THEORY SPACE

In this appendix we present the analytical expressions of zero-mode wave function overlaps in the theory space, from which follow the mass matrix elements $M_{ij}^{u,d}$ (27), (28). These expressions in turn were compiled using the exact solutions (A20), (A24) for the wave functions. In what follows we use XX to denote the overlap of two wave functions localized at the same site $n=1$, and XY the overlap of the first wave function localized at $n=1$ and the second at $n=N$. All other overlap configurations can be easily found by virtue of relation (A23).

It follows from Eqs. (27), (28) that

$$\begin{aligned}
XX &= \left(\sum_{n=1}^{N-1} x_n^{(1)*} x_n^{(2)} \right) + x_{N-1}^{(1)*} x_{N-1}^{(2)} \\
&= \frac{C_1 C_2}{4} \left(\frac{e^{(N-1)(i\theta_1 - i\theta_2 - \alpha_1 - \alpha_2)} - 1}{1 - e^{-(i\theta_1 - i\theta_2 - \alpha_1 - \alpha_2)}} e^{N(\alpha_1 + \alpha_2)} (1 - e^{-i\theta_1 - \alpha_1}) (1 - e^{i\theta_2 - \alpha_2}) \right. \\
&\quad - \frac{e^{(N-1)(i\theta_1 - i\theta_2 - \alpha_1 + \alpha_2)} - 1}{1 - e^{-(i\theta_1 - i\theta_2 - \alpha_1 + \alpha_2)}} e^{N(\alpha_1 - \alpha_2)} (1 - e^{-i\theta_1 - \alpha_1}) (1 - e^{i\theta_2 + \alpha_2}) \\
&\quad - \frac{e^{(N-1)(i\theta_1 - i\theta_2 + \alpha_1 - \alpha_2)} - 1}{1 - e^{-(i\theta_1 - i\theta_2 + \alpha_1 - \alpha_2)}} e^{N(-\alpha_1 + \alpha_2)} (1 - e^{-i\theta_1 + \alpha_1}) (1 - e^{i\theta_2 - \alpha_2}) \\
&\quad \left. + \frac{e^{(N-1)(i\theta_1 - i\theta_2 + \alpha_1 + \alpha_2)} - 1}{1 - e^{-(i\theta_1 - i\theta_2 + \alpha_1 + \alpha_2)}} e^{-N(\alpha_1 + \alpha_2)} (1 - e^{-i\theta_1 + \alpha_1}) (1 - e^{i\theta_2 + \alpha_2}) \right) \\
&\quad + C_1 C_2 e^{i(N-1)(\theta_1 - \theta_2)} \sinh \alpha_1 \sinh \alpha_2, \tag{C1}
\end{aligned}$$

$$\begin{aligned}
XY &= x_1^{(1)*} y_2^{(2)} + \left(\sum_{n=2}^{N-1} x_n^{(1)*} y_n^{(2)} \right) + x_{N-1}^{(1)*} y_N^{(2)} \\
&= C_1 C_2 e^{i\theta_1 - 2\theta_2} \left[\sinh(N-1)\alpha_1 - e^{-i\theta_1} \sinh(N-2)\alpha_1 \right] \sinh \alpha_2 \\
&\quad + \frac{C_1 C_2}{4} \left(- \frac{e^{(N-2)(i\theta_1 - i\theta_2 - \alpha_1 - \alpha_2)} - 1}{1 - e^{-(i\theta_1 - i\theta_2 - \alpha_1 - \alpha_2)}} e^{i\theta_1 - i\theta_2 - \alpha_1 - \alpha_2} e^{N\alpha_1 + \alpha_2} (1 - e^{-i\theta_1 - \alpha_1}) (1 - e^{-i\theta_2 + \alpha_2}) \right. \\
&\quad + \frac{e^{(N-2)(i\theta_1 - i\theta_2 - \alpha_1 + \alpha_2)} - 1}{1 - e^{-(i\theta_1 - i\theta_2 - \alpha_1 + \alpha_2)}} e^{i\theta_1 - i\theta_2 - \alpha_1 + \alpha_2} e^{N\alpha_1 - \alpha_2} (1 - e^{-i\theta_1 - \alpha_1}) (1 - e^{-i\theta_2 - \alpha_2}) \\
&\quad + \frac{e^{(N-2)(i\theta_1 - i\theta_2 + \alpha_1 - \alpha_2)} - 1}{1 - e^{-(i\theta_1 - i\theta_2 + \alpha_1 - \alpha_2)}} e^{i\theta_1 - i\theta_2 + \alpha_1 - \alpha_2} e^{-N\alpha_1 + \alpha_2} (1 - e^{-i\theta_1 + \alpha_1}) (1 - e^{-i\theta_2 + \alpha_2}) \\
&\quad \left. - \frac{e^{(N-2)(i\theta_1 - i\theta_2 + \alpha_1 + \alpha_2)} - 1}{1 - e^{-(i\theta_1 - i\theta_2 + \alpha_1 + \alpha_2)}} e^{i\theta_1 - i\theta_2 + \alpha_1 + \alpha_2} e^{-N\alpha_1 - \alpha_2} (1 - e^{-i\theta_1 + \alpha_1}) (1 - e^{-i\theta_2 - \alpha_2}) \right) \\
&\quad + C_1 C_2 e^{i(N-1)\theta_1 - N\theta_2} \sinh \alpha_1 \left[\sinh(N-1)\alpha_2 - e^{-i\theta_2} \sinh(N-2)\alpha_2 \right]. \tag{C2}
\end{aligned}$$

where C_1, C_2 are the normalization factors, which are determined also from the overlap of the respective wave function with itself.

APPENDIX D: NUMERICAL TABLES

TABLE I: Central values and uncertainties for the masses of the 6 quarks evaluated at M_Z , for the two ratios m_u/m_d and m_s/m_d , for the absolute values of the CKM matrix elements and the CP parameters $\bar{\rho}, \bar{\eta}$

x_i	$\langle x_i \rangle$	$ x_i^{max} - x_i^{min} /2$
m_u	2.33×10^{-3}	0.45×10^{-3}
m_c	0.685	0.061
m_t	181	13
m_d	4.69×10^{-3}	0.66×10^{-3}
m_s	0.0934	0.0130
m_b	3.00	0.11
m_u/m_d	0.497	0.119
m_s/m_d	19.9	3.9
$ V_{ud} $	0.97485	0.00075
$ V_{us} $	0.2225	0.0035
$ V_{ub} $	0.00365	0.0115
$ V_{cd} $	0.2225	0.0035
$ V_{cs} $	0.9740	0.0008
$ V_{cb} $	0.041	0.003
$ V_{td} $	0.009	0.005
$ V_{ts} $	0.0405	0.0035
$ V_{tb} $	0.99915	0.00015
$\bar{\rho}$	0.22	0.10
$\bar{\eta}$	0.35	0.05

TABLE II: 20-parameter space solutions found in 4 different cases of the model presented in Sec. IIIA (N=10 for all cases)

	(<i>QU</i> D1)	(<i>QU</i> 1 <i>DN</i>)	(<i>QU</i> <i>DN</i>)	(<i>D</i> 1 <i>QU</i> <i>N</i>)
α_{Q1}	2.290	0.208	2.311	0.215
α_{Q2}	0.007	0.236	0.011	0.251
α_{Q3}	1.497	0.220	1.656	0.213
α_{U1}	0.771	0.439	0.623	0.572
α_{U2}	0.759	1.900	0.603	0.823
α_{U3}	0.927	0.433	0.722	0.745
α_{D1}	0.829	0.027	0.794	0.541
α_{D2}	0.535	0.022	0.471	0.057
α_{D3}	1.123	0.029	1.105	0.022
θ_{Q1}	1.002	0.974	1.234	0.959
θ_{Q2}	3.862	0.983	4.702	0.958
θ_{Q3}	1.678	0.989	1.999	0.965
θ_{U1}	1.163	1.407	1.276	0.197
θ_{U2}	1.100	14.78	1.246	13.67
θ_{U3}	1.247	-5.290	1.420	-5.52
θ_{D1}	-0.204	-0.535	-0.135	-0.182
θ_{D2}	3.098	4.715	2.809	3.471
θ_{D3}	0.086	9.645	-0.174	9.499
$\kappa_{UV}/\sqrt{2}$	78.37	66.63	78.36	71.21
$\kappa_{DV}/\sqrt{2}$	1.35	23.24	1.37	26.48

[1] N. Arkani-Hamed, A. G. Cohen and H. Georgi, Phys. Rev. Lett. **86**, 4757 (2001).

[2] C. T. Hill, S. Pokorski and J. Wang, Phys. Rev. D **64**, 105005 (2001).

- [3] N. Jackiw and S. Rebbi, Phys. Rev. D **13**, 3398 (1976).
- [4] N. Arkani-Hamed and M. Schmaltz, Phys. Rev. D **61**, 033005 (2000)
- [5] P. Q. Hung and N-K. Tran, Phys. Rev. D **69**, 064003 (2004).
- [6] N. Cosme, J. M. Frere and L. L. Honorez, Phys. Rev. D **68**, 096001 (2003).
- [7] N. Cosme and J. M. Frere, Phys. Rev. D **69**, 036003 (2004).
- [8] B. Gdzadkowski and J. Wudka, hep-ph/0401232.
- [9] Y. Hosotani, Phys. Lett. B **129**, 193 (1983).
- [10] E. A. Mirabelli and M. Schmaltz, Phys. Rev. D **61**, 113011 (2000).
- [11] G. C. Branco, A. De Gouvea and M. N. Rebelo, Phys. Lett. B **506**, 115 (2001).
- [12] A. Soddu and N-K. Tran, Phys. Rev. D **69**, 015010 (2004).
- [13] W. Skiba and D. Smith, Phys. Rev. D **65**, 095002 (2002).
- [14] C. T. Hill and A. Leibovich, Phys. Rev. D **66**, 016006 (2002).
- [15] H. Abe, T. Kobayashi, N. Maru and K. Yoshioka Phys. Rev. D **67**, 045019 (2003).
- [16] P. Q. Hung and N-K. Tran, Phys. Rev. D **70**, 126014 (2004).
- [17] P. Q. Hung and M. Seco, Nucl. Phys. B **653**, 123 (2003).
- [18] P. Q. Hung, M. Seco and A. Soddu, Nucl. Phys. B **692**, 83 (2004).
- [19] S. Nojiri, S. D. Odintsov and A. Sugamoto, Phys. Lett. B **590**, 239 (2004).
- [20] S. Kirkpatrick, C. D. Gelatt and M. P. Vecchi, Science **220**, 671 (1983); S. Kirkpatrick, J. Stat. Phys. **34**, 975 (1984); N. Metropolis, A. Rosenbluth. M. Rosenbluth, A. Teller and E. Teller, J. Chem. Phys. **21**, 1087 (1953).
- [21] W. H. Press, S. A. Teukolosky, W. T. Vetterling and B. P. Flannery, *Numerical Recipes in C*, 2nd ed. (Cambridge University Press, New York, 1992).
- [22] F. Bauer, M. Lindner and G. Seidl, J. High Energy Phys. **0405**, 026 (2004).
- [23] A. Delgado, A. Pomarol and M. Quiros, J. High Energy Phys. **0001**, 030 (2000).
- [24] I. S. Gradshteyn and I. M. Ryzhik, Tables of Integrals, Series and Products, 5th ed. (Academic Press, Boston, 1994).
- [25] Another somewhat simpler solution of the above equation set is presented in [16]
- [26] The finiteness of 1-loop effective potential requires the mass of fermionic tower be trigonometric function of the mode number [14]. In the continuum limit such as in a “ S^1/Z_2 ” compactification, the orbifold boundary conditions (2) can fulfill this requirement.